Ludden, J.N., Plank, T., and Escutia, C. (Eds.)
Proceedings of the Ocean Drilling Program, Scientific Results Volume 185

7. Pleistocene Deep-Sea Sediment in ODP Hole 1149A, Nadezhda Basin: Sources, Alteration, and Age Controls (0–800 ka)[1]

Michael Urbat[2] and Thomas Pletsch[3]

ABSTRACT

We employed several approaches to refine age estimates for the late Pleistocene sedimentary section recovered from Ocean Drilling Program Hole 1149A, which is located in the abyssal plain of the Nadezhda Basin in the northwest Pacific Ocean. Our study is based on a combination of paleo- and rock magnetic as well as geochemical-mineralogic X-ray fluorescence and X-ray diffraction data measured on 300 pairs of samples. These were taken at high resolution (1 sample per 3–5 k.y.) from the uppermost 32 m in Hole 1149A, which covers the Brunhes Chron and extends into the Matuyama Chron. This section provides an expanded record of eolian dust (supplied from the Asian continent), of changing volcanic ash input, and of siliceous plankton accumulation, with recurrent diagenetic intervals in a deep-sea environment. We used normative calculations on the basis of Al and Cr contents to discriminate between the major groups of components (terrigenous, volcanogenic, biogenic, and diagenetic) in combination with our magnetic results. The magnetic signal in Hole 1149A is driven dominantly by the varying inputs of eolian dispersed ash and terrigenous dust. A glacial–interglacial influence on the record is established by a correlation of the CaO record from Hole 1149A to the SPECMAP $\delta^{18}O$ composite curve. Despite the generally excellent paleomagnetic properties of the sediment, there is no record of polarity events during the Brunhes Chron to

[1]Urbat, M., and Pletsch, T., 2003. Pleistocene deep-sea sediment in ODP Hole 1149A, Nadezhda Basin: sources, alteration, and age controls (0–800 ka). *In* Ludden, J.N., Plank, T., and Escutia, C. (Eds.), *Proc. ODP, Sci. Results,* 185, 1–21 [Online]. Available from World Wide Web: <http://www-odp.tamu.edu/publications/185_SR/VOLUME/CHAPTERS/012.PDF>. [Cited YYYY-MM-DD]
[2]Department of Geology, University of Cologne, Zülpicherstrasse 49a, 50674 Köln, Germany. **m.urbat@uni-koeln.de**
[3]Bundesanstalt für Geowissenschaften und Rohstoffe (BGR), Stilleweg 2, 30655 Hannover, Germany.

Initial receipt: 16 January 2002
Acceptance: 5 February 2003
Web publication: 29 September 2003
Ms 185SR-012

allow construction of further age tie points nor is the record suitable for relative paleointensity stratigraphy. Several intervals are characterized by dramatic changes in rock magnetic parameters and adjacent enrichments in diagenetic minerals. These intervals correspond to paleoredox boundaries, where suboxic conditions promoted the destruction of the primary magnetic signal and the precipitation of rhodochrosite ($MnCO_3$).

INTRODUCTION

Hole 1149A (Ocean Drilling Program [ODP] Leg 185) (Plank, Ludden, Escutia, et al., 2000) is located at 31°N latitude, ~100 km east of the Izu-Bonin Trench on the Pacific plate in the Nadezhda Basin, southeast of Japan. One of the objectives of Leg 185 was to characterize the sedimentation history, including volcanic ashes of the upper 120-m section of Hole 1149A. This section provides an expanded record of eolian dust supply from the Asian continent, siliceous plankton accumulation, and varying contributions of both discrete ash layers and dispersed ash to a truly deep-sea environment since the late Miocene (Plank, Ludden, Escutia et al., 2000). During deposition of the Miocene–Holocene, sediment at the site (water depth = 6000 m) was continuously below the carbonate compensation depth (CCD). The sedimentary section is thus free of pelagic carbonate and was also beyond the reach of turbidite input, being sheltered off by the Japan Trench (Fig. **F1**). The section consists of multicolored, heavily bioturbated clays and silts with variable concentrations of terrigenous clay and silt, siliceous microfossils, dispersed volcanic ash, and intercalated discrete ash layers. In spite of the absence of turbidites and pelagic carbonate, sediment accumulation rates range from 0.4 g/cm²/k.y. at the bottom of the section (6–6.5 Ma) to 2.4 g/cm²/k.y. during the Brunhes Chron (0.8 Ma–present). Increasing accumulation rates are thought to mainly result from the plate tectonic movement of the drill site toward the siliciclastic and volcanic source areas (Plank, Ludden, Escutia, et al., 2000). The sediment supply at Site 1149 is restricted to the three sources: eolian dust from the Asian continent and possibly Japan, dispersed and discrete volcanic ash from the Japanese Island arc, and biogenic opal from surface waters.

In this paper, we discuss a refined time frame for the last 800 k.y. of sediment accumulation history in Hole 1149A based on magnetic, geochemical, and mineralogic results. This age model forms the grounds for a more detailed interpretation of the continental and oceanic environmental controls on the abyssal northwest Pacific Ocean during and slightly beyond the Brunhes Chron, which will be the focus of a subsequent paper.

Based on the high-quality magnetostratigraphic records obtained during Leg 185 (Shipboard Scientific Party, 2000), the Brunhes/Matuyama (B/M) boundary is at 26.3 meters below seafloor (mbsf). Given the pelagic turbidite-free depositional environment, we intended to refine the magnetostratigraphy using the ages of well-established polarity events during the Brunhes Chron (Langereis et al., 1997; Nowaczyk and Antonow, 1997). We also intended to extract a relative paleointensity (RPI) record from the sampled interval (e.g., Tauxe, 1993) and use it for paleointensity stratigraphy (see **"Discussion,"** p. 7). Hole 1149A seemed to have a potentially meaningful RPI record, considering the monotonous terrestrial dust supply confirmed by our mineralogical measurements. Before attempting any such interpretation,

F1. Climate/ocean system in the northwest Pacific, p. 11.

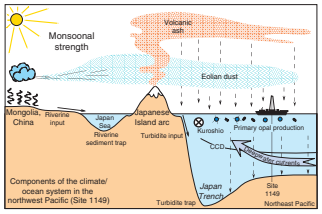

we first sought to establish the influence of the volcanic ash and/or postdepositional alteration on the sediment magnetic properties. As a result, neither the RPI nor polarity events proved to be robust enough to use for age refinement.

METHODS

Pilot samples of ~50 cm^3 were taken at a spacing of one per section aboard the *JOIDES Resolution* to test our methodology and to separate enough coarse grains for future analyses. The main sample set, which was taken at the ODP Gulf Coast Core Repository, consists of two subsamples collected every 10 cm throughout the upper 32 mbsf. One set of subsamples were collected in oriented 8-cm^3 plastic cubes (used for magnetic measurements), kept in an airtight box, and stored at 4°C in a refrigerator to prevent sample alteration. When the magnetic measurements were completed, these subsamples were air dried below 50°C and softly ground with an agate mortar and pestle for X-ray diffraction (XRD) and X-ray fluorescence (XRF) analyses. The other subsamples were collected in 10-cm^3 push tubes that were directly air-dried and split, with one split suspended in demineralized water. Where the magnetic measurements took longer than anticipated, untreated splits from the push tubes were prepared for XRD and XRF as described above.

Using the tentative shipboard identification of the B/M boundary and under the assumption of constant sediment accumulation rates during the Brunhes Chron of 2.4 g/cm^2/k.y., accordingly (Shipboard Scientific Party, 2000), we sampled the uppermost 32 m of Hole 1149A at a quasiconstant rate of 3–5 k.y. from the working halves of Sections 185-1149A-1H-1, 10 cm, through 4H-5, 138 cm.

All magnetic measurements were carried out at the Paleomagnetic Laboratory, Department of Geology, University of Cologne. Natural remanent magnetization (NRM) intensities were measured on a three-axis 2-G Enterprises direct-current superconducting quantum interference device (DC-SQUID) magnetometer model 755R designed to measure discrete specimens. The instrument features in-line alternating-field (AF) solenoids for stepwise sample demagnetization, anhysteretic remanent magnetization (ARM), and isothermal remanent magnetization (IRM).

Three-axis static AF demagnetization up to 100 mT was used to determine the characteristic remanent magnetization (ChRM) for all samples from the paleomagnetic set. Volume susceptibility (κ) and anisotropy of magnetic susceptibility (AMS) were measured at room temperature in a KLY-2 susceptibility bridge (AGICO, Czech Republic). ARM was imparted perpendicular to the bedding plane (100-mT AF peak; 50-μT DC bias field parallel to AF). Pilot samples with varying AF peaks showed that ARM intensity after the 100-mT AF peak is the maximum intensity that can be imparted in the samples. All ARMs were demagnetized at the 15-mT level in order to obtain a simple normalizer to the NRM that might serve as a relative RPI. IRMs were imparted on the samples using the in-line pulse magnetizer of the SQUID magnetometer—stepwise, up to 1.5 T for selected samples or in a single step for the remainder of the sample set. Stepwise backfield IRM to 300 mT was imparted in all samples in order to calculate the *S* ratio (Bloemendal et al., 1993) and coercivity of remanence (B_{cr}) IRM intensities of ~50% of the sample set were determined using a Molspin magnetometer (Molspin Ltd., United Kingdom) because they exceeded the dynamic range of the SQUID magne-

tometer. Instrument output compatibility was assured using a calibration constant determined on samples that could be measured on both magnetometers.

Low- and high-temperature susceptibilities (–192° to 700°C) of selected samples were determined using the Kappabridge KLY-2 in combination with the CS23 low-temperature apparatus and the CS23 furnace apparatus (AGICO). Instrument-specific standard procedures were applied.

XRD was carried out on untreated bulk powders that were backfilled into standard aluminium sample holders. Measurements were performed on a Philips PW 1800 with a Cu tube and a Ni monochromator using the following settings: 40-kV/40-mA acceleration voltage/anode current, automatic divergence slit, and sample spinner off. All samples were scanned from 2° to 60°2θ with 1 s per step of 0.02°2θ. Interpretations and peak measurements of the resulting X-ray diffractograms were performed utilizing MacDiff Software version 4.2 by Reiner Petschick (Petschick, 2000).

XRF analyses were conducted at the Geochemical Laboratory, University of Hamburg, Germany. Loss on ignition (LOI), which includes H_2O, CO_2, F, Cl, S, and CH_4 as well as the oxidation gain of Fe, Mn, and other elements, was determined by heating the sample splits at 1000°C for 1 hr. Element concentrations were recalculated according to oxidation and LOI.

Spectral analysis of the data (Lomb-Scargle Fourier Transformation) (Lomb, 1976; Scargle, 1982) was performed using the in-house software SPECLAB (G. Port) that was written at and is routinely used at the University of Cologne.

Spectral analysis of downhole properties is best conducted on data from a continuous depth section without overlapping sections or major voids. The studied sediment cores displayed a significant amount of overlap, most probably as a result of core expansion related to decompression after recovery. No voids or empty sections were present in the studied interval, although some coring gaps are possible between cores. Because the sedimentary section was only cored in a single hole, the amount of missing or duplicated section cannot be established. We suspect the amount is insignificant. To arrive at a nearly continuous depth section, we concatenated the recovered core lengths and added the depth shift downward to the depths assigned on board (mbsf). All subsequent depth assignments will be reported as meters recovered section (mrs), accordingly. The depths shifts are 0 m for Core 185-1149A-1H; 0.02 m for Core 2H; 0.46 m for Core 3H; and 0.76 m for Core 4H.

RESULTS

Petrography

The Pleistocene section of Hole 1149A consists of multicolored clayey silts and silty clays with variable concentrations of terrigenous material, dispersed volcanic ash, siliceous microfossils, and intercalated ash layers. Sand content of the background sediment (i.e., excluding discrete ash layers) ranges from 0% to ~15% and mostly consists of ash particles. The mineral composition of the background sediment varies little. According to these initial results, the components were lumped into four major groups (Fig. F2). The terrigenous (Ter) group consists of quartz, feldspars, and primary clay minerals. The volcanogenic (Vol)

F2. Normative calculations on the basis of the geochemical results, p. 12.

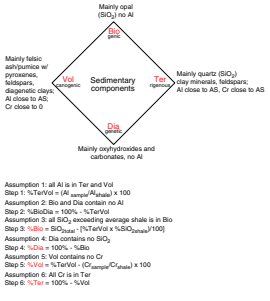

group consists mainly of felsic ash and pumice, pyroxenes, feldspars, and diagenetic clay minerals. The biogenic (Bio) group consists exclusively of opaline silica. The diagenetic (Dia) group comprises Fe and Mn oxyhydroxides and rhodochrosite ($MnCO_3$). It is important to note that we did not include any silicates (i.e., clay minerals) in the diagenetic group. These silicates likely formed from volcanic and/or terrigenous precursors, and we consider them part of the respective component fluxes to the seafloor.

Geochemistry

We used simple normative calculations on the basis of Al, SiO_2, and Cr contents to discriminate between the major groups of components (Ter, Vol, Bio, and Dia) (Fig. F2). First, we assumed that all Al is incorporated in Ter and Vol components, which have Al concentrations similar to average shale (Al = 8.84%) (Chester, 1990) and that Bio and Dia components do not contain any Al. Second, we assumed that all SiO_2 exceeding average shale belongs to the Bio components and that the Dia components do not contain any SiO_2. This assumption seems warranted because none of the analyzed samples exceeds the SiO_2 concentration of an average shale (SiO_2 = 58.9%) (Chester, 1990). Third, we assumed that all Cr is in the Ter components and that the Vol components do not contain any Cr. Finally, we assumed that the Al and Cr concentrations in the respective components correspond to the concentrations of these elements in an average shale. The latter assumption seems warranted because the purest discrete ash layers contain only very low concentrations of Cr (0–4 ppm) and only one sample exceeds the Cr concentration of average shale (110 ppm) (Taylor and McLennan, 1985; Peters et al., 2000).

According to this model, concentrations in background sediments (excluding discrete ash layers) fluctuate around the following means: eolian dust = 47% (σ = 11%); dispersed ash = 41% (σ = 10%); and biogenic silica = 12% (σ = 5%).

Composition of the Magnetic Signal

Magnetomineralogical measurements of the sampled section show homogenous rock magnetic properties downhole. The monotonous record is only interrupted by several meter-scale distinct drops in magnetization intensities of both natural and laboratory-induced magnetizations (NRM, κ, ARM, and IRM) and concomitant changes in magnetic parameters sensitive to magnetic mineralogy and grain size (Fig. F3).

NRM intensities in Figure F3 are reported at the 15-mT demagnetization level, at which possible drilling-induced or viscous magnetizations are removed from the samples (see "Paleomagnetism," p. 7). Intensities in the sampled section in Hole 1149A span more than two orders of magnitude, ranging from <1 to 500 mA/m. The large range is due to several low-intensity intervals, the most prominent of which are around 4, 12, 21, 27, and 30.5 mrs. The remainder of the section, hereafter referred to as background sediment, displays a more restricted variability of only 30–100 mA/m. Volume magnetic susceptibilities (κ [100–5000 μSI; background sediment = 300–2000 μSI], ARM [10–1200 mA/m; background = 100–500 mA/m], and IRM [1.2–170 A/m; background = 10–60 A/m]) all mimic the general downhole behavior of the NRM, although a somewhat lower variability in the background is seen in Fig-

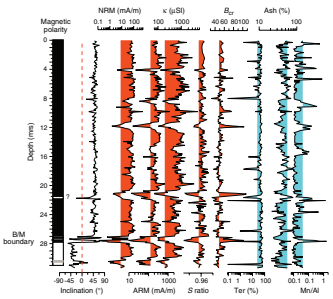

F3. Downhole plot of paleomagnetic and geochemical results, p. 13.

ure F3. Linear regressions calculated from the data yield coefficients of R^2 above 0.8 for all respective correlations, an example biplot of which is shown in Figure F4 for κ vs. IRM.

The remanent magnetic signal in Hole 1149A is carried by the low-coercivity mineral magnetite. This is confirmed by IRM acquisition (Fig. F5) and backfield measurements as well as low- and high-temperature susceptibility curves (Fig. F6). IRM saturation in the background sediment is typically reached between 200 and 300 mT, which is higher than would be expected for pure magnetite (<200 mT). We attribute this behavior to a slight oxidation of the iron oxide. Low- and high-temperature susceptibility measurements confirm the dominance of slightly oxidized magnetite with respective distinct changes in magnetization corresponding to the Verwey transition at –160°C (Özdemir et al., 1993) and the Curie temperature at 550°–580°C, respectively (Fig. F6). The remanent magnetic properties of the discrete ash layers (Fig. F3) do not appear to differ qualitatively from the bulk of the sediment, although they do vary slightly in relative quantity of magnetic minerals. Only the low-intensity zones recognized from the concentration-dependent parameters (CDPs) display different magnetic properties. Remanent coercivities (B_{cr}), which vary between 40 and 50 mT in the background sediment, are in excess of 100 mT in these intervals (Fig. F3). IRM acquisition curves confirm the higher coercivity properties in these intervals, and saturation is only reached at fields >500 mT (Fig. F5). *S* ratios calculated from the backfield measurements drop to values around 0.85 as opposed to the remainder of the intervals, where values are centered around 0.96 (again confirming magnetite) (Fig. F3). Unfortunately, the low-temperature measurements gave spurious results in these intervals because of the small remanent intensities and susceptibility results appear to be dominated by the paramagnetic components of the sediment (e.g., clay minerals).

In the deep-sea setting at Site 1149, we expected the contents of magnetic minerals to be driven by eolian input (i.e., variations in terrestrial dust with possible contributions from dispersed ash forming the pelagic rain in this environment). We tested this hypothesis by correlation of the background magnetic signal (i.e., having excluded the low-intensity intervals) to the extracted terrigenous or ash components of the sediment (see "Geochemistry," p. 5). Linear regression coefficients calculated for various combinations of CDPs vs. the four major sediment components (Ter, Vol, Bio, and Dia) (Fig. F2) or single geochemical components (e.g., Si, Ti, Cr, Al, etc.) indicate that there is no significant match in any case (R^2 < 0.1), except for a weak correlation of CDP vs. Ter and a positive correlation to the ash component. Interestingly, there is, however, a strong correlation of CDPs to CaO (R^2 = 0.6). Our measurements indicate that Ca is mainly contained in minerals associated with the dispersed ash (CaO vs. dispersed ash yields; R^2 = 0.6) (Fig. F4), and we therefore conclude that the magnetic signal in Hole 1149A is mainly driven by varying contributions of dispersed ash rather than the terrigenous dust component. Hence, magnetite must be equally associated with dispersed ash rather than the dust component. The less obvious correlation of CDP to the extracted ash component of the sediment may be due to extremely low variability of the extracted ash or Ter components in the background signal. Ongoing analyses will clarify the exact role of CaO in the sediment.

F4. Bivariate scatter plots, p. 14.

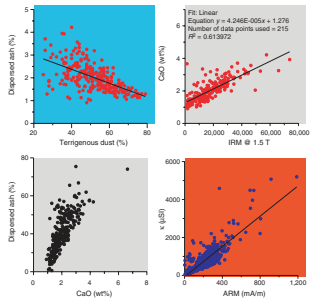

F5. Examples of IRM acquisition and backfield measurements, p. 15.

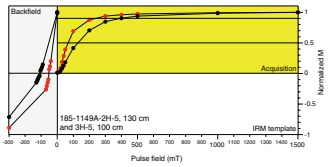

F6. Sample 185-1149A-3H-2, 100 cm, p. 16.

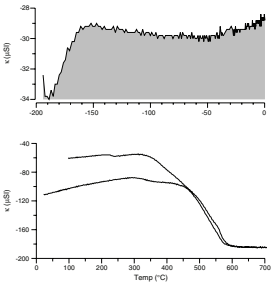

Paleomagnetism

NRM demagnetization diagrams show univectorial decay to the origin after removal of viscous and supposedly drilling-induced components at 10- to 15-mT AF. Samples dominantly conform to the expected mean value of the geocentric axial dipole for the site (cf., Shipboard Scientific Party, 2000). The Brunhes Chron to the top of the Matuyama Chron is clearly defined (Fig. F7). Placement of the B/M boundary is not straightforward at first sight, however, because after a first swing to shallow negative inclinations at 27.04 mrs, the ChRM directions swing back to positive inclinations twice (at 27.1 and 27.5) mbsf (Fig. F8). Those two intervals have, however, clearly been remagnetized during the Brunhes Chron. First, the analysis of the rock magnetic properties indicates that the interval between 26 and 28 mrs is characterized by a substantial drop in magnetic mineral concentration (CDP). Concentrations are lowest in the two positive polarity intervals. Second, magnetic mineralogy is dominantly composed of a high-coercivity mineral instead of the otherwise prevailing magnetite in the remainder of the sampled section. Third, the geochemical and mineralogical analyses indicate a concomitant change in diagenetic minerals (e.g., manganese concentration [rhodochrosite] in this interval). This indicates postdepositional alteration of at least part of the minerals at these depths that is possibly due to paleoredox changes. Three more intervals during the Brunhes Chron at Site 1149 are characterized by similar events at 4, 12, and 21 mrs. With respect to the B/M boundary at Site 1149, it appears that the polarity switch, by chance, coincided with changes in the depositional environment that triggered diagenetic alteration. We picked the B/M boundary at 27 mrs under the assumption that the shallow inclination is a consequence of newly formed magnetic minerals and alteration that did not proceed into complete remagnetization. The boundary was chosen intermediate between the last positive and this first shallow negative sample.

Polarity events during the Brunhes Chron cannot be clearly identified in Hole 1149A. Trends to negative inclinations are recorded in single samples, none of which are associated with concomitant declination swings, however. Furthermore, all these samples are either located near core or section boundaries, where potential destruction of the magnetic fabric may have occurred in the course of cutting the cores.

F7. Intensity of NRM, inclination, and declination, p. 17.

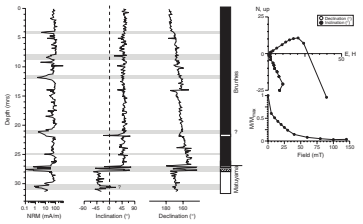

F8. Details of the inclination, ARM, and Mn/Al across the B/M boundary, p. 18.

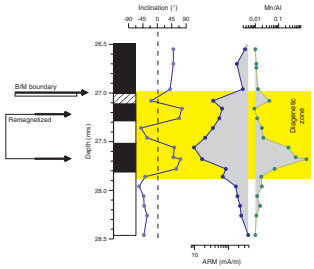

DISCUSSION

Our attempts to refine the age scale within the Brunhes Chron interval in Hole 1149A using a magnetostratigraphic approach were only partly successful. The B/M boundary can be clearly defined at 27.04 mrs, placing an age datum of 780 ka at this depth. Polarity events during the late Pleistocene, however, are not unambiguously recorded in the sediment (Fig. F7). A polarity excursion cannot be ruled out completely for Sample 185-1149A-3H-6, 9 cm, at 21.5 mrs (Fig. F3). The sample has a shallow negative inclination, which is not associated with a concomitant declination swing, however. But the sample is located in one of the suspect diagenetic zones and may well have been remagnetized during a polarity excursion.

Taking the B/M boundary at 27.04 mrs, an average sedimentation rate of 3.47 cm/k.y. can be calculated for the late Pleistocene interval in

Hole 1149A. Spectral analysis of the background sediment data (we used various XRF data, including Al, Si, Ti, and Fe) indicates strongest power in the eccentricity band (100 k.y.) (Fig. F9); there is, however, a number (>10) of almost equally strong peaks at various frequencies that cannot be identified as orbital frequencies or as first-order subharmonics. A better picture (i.e., power in both eccentricity and precession band and, hence, reducing the unidentified peaks) is obtained by decreasing the constant sedimentation rate to 2.71 cm/k.y. This, however, is in conflict with the identification of the B/M boundary. To overcome these problems, we attempted to refine the age estimates using RPI.

The RPI of the geomagnetic field has been successfully established for various marine sedimentary environments, including the North Pacific Ocean (e.g., Schneider and Mello, 1996; Roberts et al., 1997; Yamazaki, 1999). Based on empirical evidence, a number of criteria for uniformity of the magnetomineralogy need to be satisfied in order to extract a reliable RPI record from marine sediments (Tauxe, 1993; King et al., 1983). Our paleo- and rock magnetic results indicate that all of the proposed criteria are only satisfied if the low-intensity zones and the discrete ash layers are excluded. Omitting these latter intervals, however, removes a substantial amount of the record (e.g., Fig. F10) and the obtained RPI curve is not very complete. We therefore discarded any further attempts to use RPI.

The best confirmation of 100-k.y. cycles that control the eolian input in Hole 1149A comes from a correlation of the CaO data to the SPECMAP $\delta^{18}O$ curve (Imbrie et al., 1984) (Fig. F10). CaO mirrors the SPECMAP curve reasonably well, including relative amplitudes and even the baseline shift seen at ages > 400 ka. The CaO record appears to mirror variations in (eolian) dispersed ash deposition, and it appears to be modulated only to a minor extent by diagenesis or discrete ash layers. The correlation and respective depth-time conversion presented in Figure F10 yields only minor changes to the average sedimentation rate of 3.47 cm/k.y. downhole, the results of which are shown in Figure F11.

Figure F10 indicates that terrigenous dust and dispersed ash mutually supplant on a glacial–interglacial scale. Dispersed ash dominates in interglacial stages, whereas the dust supply from the Asian continent was dominant during glacial stages. This suggests changes of the (eolian) source area as a function of variations in the (monsoonal) wind pattern. Diagenetic events identified throughout Hole 1149A are prominent during glacial stages (Fig. F10) and could be related to changes in the ocean water circulation (Kuroshio Current) and concomitant precipitation variations. We plan to explore this topic in more detail in the future.

The deposition of discrete ash layers is unrelated to paleoclimatic changes, although there is a tendency of deposition during interglacial stages (Fig. F10).

CONCLUSIONS

The mutually beneficial analyses of paleomagnetic, rock magnetic, and mineralogic geochemical data suggest a 100-k.y. cyclicity in the deposition of eolian sediment components in deep-sea Hole 1149A during the last 800,000 yr. Dispersed ash and terrigenous dust are inversely correlated and mutually supplant in glacial–interglacial intervals. The primary magnetic signal is dominantly related to eolian volcanic ash

F9. Spectral analysis of Al, p. 19.

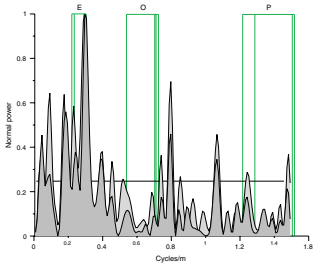

F10. The correlation of the CaO record to SPECMAP, p. 20.

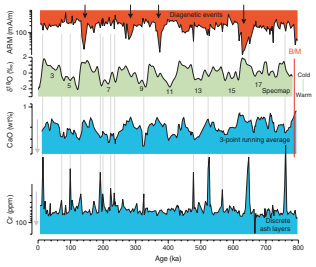

F11. Average sedimentation rates, p. 21.

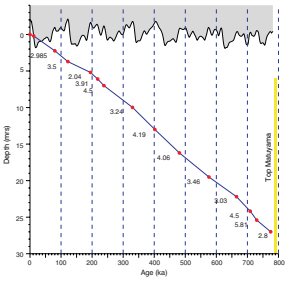

deposition rather than terrigenous dust. The B/M boundary is identified at 27.04 mrs, confirming shipboard results, although this interval is strongly altered by diagenesis, leading to remagnetization and delayed NRM acquisition. Several intervals throughout the Brunhes Chron in Hole 1149A indicate such strong diagenetic alteration of the sediment, with concomitant substantial changes of the magnetic mineralogy and occurence of Mn minerals (rhodochrosite). These intervals are present in glacial stages and appear to be related to paleoredox changes in the sediment column as a function of changing ocean water circulation.

ACKNOWLEDGMENTS

This research used samples provided by the Ocean Drilling Program (ODP). The ODP is sponsored by the U.S. National Science Foundation (NSF) and participating countries under management of Joint Oceanographic Institutions (JOI), Inc. Funding for this research was provided by the Deutsche Forschungsgemeinschaft grant UR74/2 to Michael Urbat. Discussions with Peter Hofmann improved the manuscript. Alexander Weingarten and Mathias Höcker carried out the magnetic measurements. Reviews by Gary Acton and an anonymous reviewer are very much appreciated.

REFERENCES

Bloemendal, J., King, J.W., Hunt, A., deMenocal, P.B., and Hayashida, A., 1993. Origin of the sedimentary magnetic record at Ocean Drilling Program sites on the Owen Ridge, western Arabian Sea. *J. Geophys. Res.,* 98:4199–4219.

Chester, R., 1990. *Marine Geochemistry:* London (Unwin Hyman).

Imbrie, J., Hays, J.D., Martinson, D.G., McIntyre, A., Mix, A.C., Morley, J.J., Pisias, N.G., Prell, W.L., and Shackleton, N.J., 1984. The orbital theory of Pleistocene climate: support from a revised chronology of the marine $\delta^{18}O$ record. *In* Berger, A., Imbrie, J., Hays, J., Kukla, G., and Saltzman, B. (Eds.), *Milankovitch and Climate* (Pt. 1), NATO ASI Ser. C, Math Phys. Sci., 126:269–305.

King, J.W., Banerjee, S.K., and Marvin, J., 1983. A new rock-magnetic approach to selecting sediments for geomagnetic paleointensity studies: application to paleointensity for the last 4000 years. *J. Geophys. Res.,* 88:5911–5921.

Langereis, C.G., Dekkers, M.J., de Lange, G.J., Paterne, M., and Santfoort, P.J.M., 1997. Magnetostratigraphy and astronomical calibration of the last 1.1 Myr from an eastern Mediterranean piston core and dating of short events in the Brunhes Chron. *Geophys. J. Int.,* 129:75–94.

Lomb, N.R., 1976. Least-squares frequency analysis of unequally spaced data. *Astophys. Space Sci.,* 39:447–462.

Nowaczyk, N., and Antonow, M., 1997. High-resolution magnetostratigraphy of four sediment cores from the Greenland Sea: identification of the Mono Lake excursion, Laschamp and Biwa I/Jamaica geomagnetic polarity events. *Geophys. J. Int.,* 131:310–324.

Özdemir, Ö., Dunlop, D.J., and Moskowitz, B.M., 1993. The effect of oxydation on the Verwey transition in magnetite. *Geophys. Res. Lett.,* 20:1671–1674.

Peters, J.L., Murray, R.W., Sparks, J.W., and Coleman, D.S., 2000. Terrigenous matter and dispersed ash in sediment from the Caribbean Sea: results from Leg 165. *In* Leckie, R.M., Sigurdsson, H., Acton, G.D., and Draper, G. (Eds.), *Proc. ODP, Sci. Results,* 165: College Station, TX (Ocean Drilling Program), 115–124.

Petschik, R. 2000. MacDiff 4.2 Manual. *MacDiff* [Online]. Available from World Wide Web: <http://www.geologie.uni-frankfurt.de/Staff/Homepages/Petschick/RainerE.html>. [Revised 2001-05-17]

Plank, T., Ludden, J.N., Escutia, C., et al., 2000. *Proc. ODP, Init. Repts.,* 185 [CD-ROM]. Available from: Ocean Drilling Program, Texas A&M University, College Station TX 77845-9547, USA.

Roberts, A.P., Lehman, B., Weeks, R.J., Verosub, K.L., and Laj, C., 1997. Relative paleointensity of the geomagnetic field over the last 200,000 years from ODP Sites 883 and 884, North Pacific Ocean. *Earth Planet. Sci. Lett.,* 152:11–23.

Scargle, J.D., 1982. Studies in astronomical time series analysis II. Statistical aspects of spectral analysis of unevenly spaced data. *Astron. J.,* 263:835–853.

Schneider, D.A., and Mello, G.A., 1996. A high-resolution marine sedimentary record of geomagnetic intensity during the Brunhes Chron. *Earth Planet. Sci. Lett.,* 144:297–314.

Shipboard Scientific Party, 2000. Site 1149. *In* Plank, T., Ludden, J.N., Escutia, C., et al., *Proc. ODP, Init. Repts.,* 185, 1–190 [CD-ROM]. Available from: Ocean Drilling Program, Texas A&M University, College Station TX 77845-9547, USA.

Tauxe, L., 1993. Sedimentary records of relative paleointensity of the geomagnetic field: theory and practice. *Rev. Geophys.,* 31:319–354.

Taylor, S.R., and McLennan, S.M., 1985. *The Continental Crust: Its Composition and Evolution:* Oxford (Blackwell Scientific).

Yamazaki, T., 1999. Relative paleointensity of the geomagnetic field during Brunhes Chron recorded in North Pacific deep-sea sediment cores: orbital influence? *Earth Planet. Sci. Lett.,* 169:23–35.

Figure F1. Cartoon summarizing the components of the climate/ocean system in the northwest Pacific (ODP Site 1149), with sediment sources including eolian dust, volcanic ash, and biogenic production. Deposition in Hole 1149A is uninfluenced by turbidites or riverine input. The dominant ocean current is the Kuroshio. CCD = carbonate compensation depth.

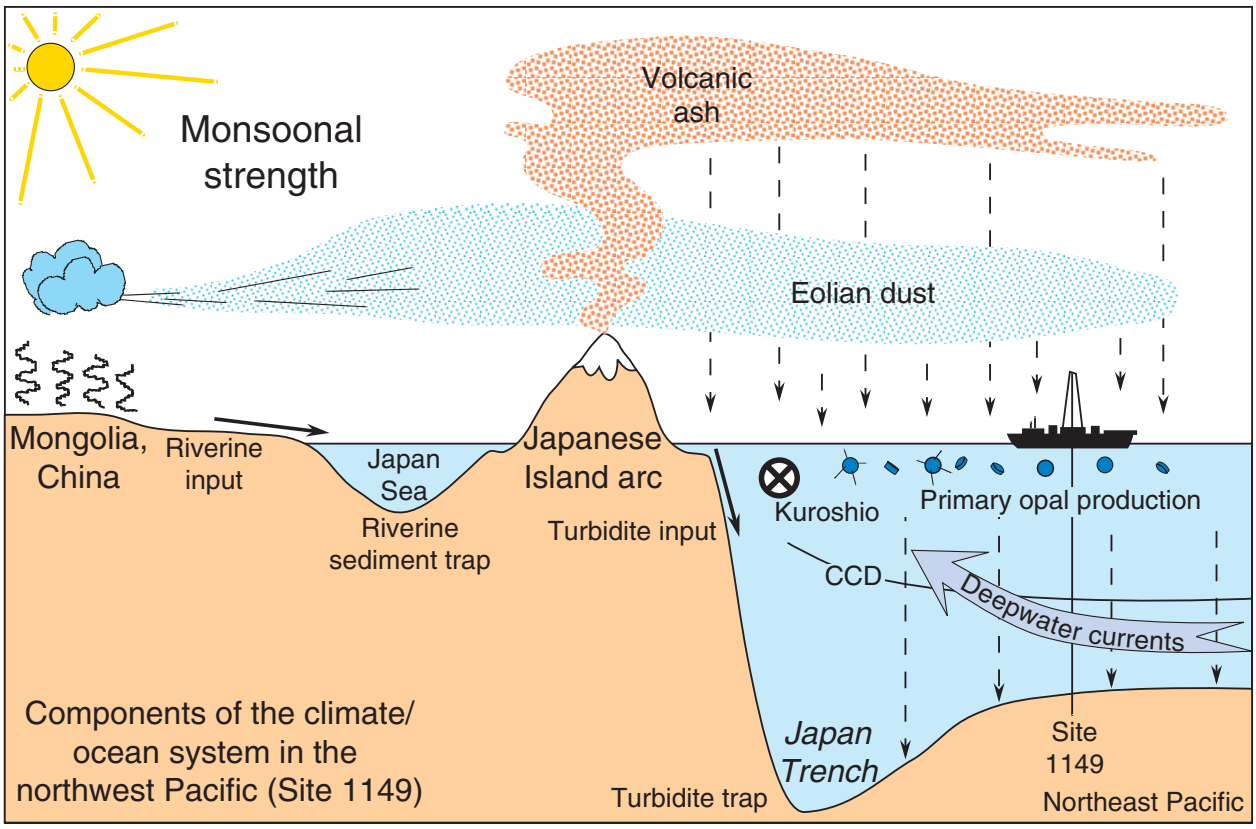

Figure F2. Simple normative calculations on the basis of the geochemical results discriminate four major sedimentary components. AS = average shale.

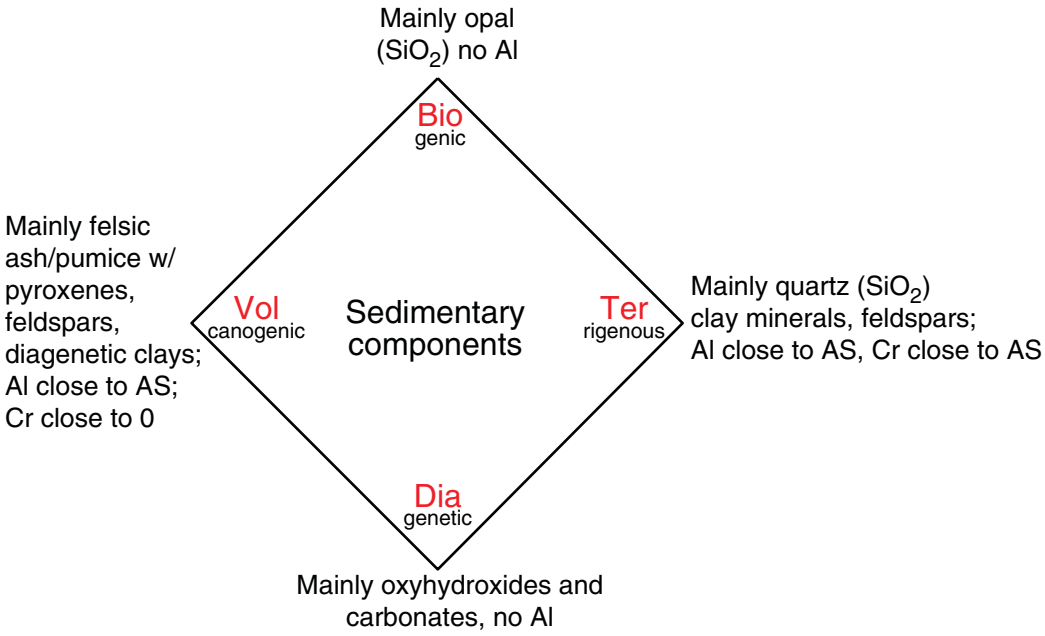

Assumption 1: all Al is in Ter and Vol
Step 1: %TerVol = (Al_{sample}/Al_{shale}) x 100
Assumption 2: Bio and Dia contain no Al
Step 2: %BioDia = 100% - %TerVol
Assumption 3: all SiO_2 exceeding average shale is in Bio
Step 3: %Bio = SiO_{2total} - [%TerVol x $\%SiO_{2shale}$)/100]
Assumption 4: Dia contains no SiO_2
Step 4: %Dia = 100% - %Bio
Assumption 5: Vol contains no Cr
Step 5: %Vol = %TerVol - (Cr_{sample}/Cr_{shale}) x 100
Assumption 6: All Cr is in Ter
Step 6: %Ter = 100% - %Vol

Figure F3. Downhole plot comprising selected paleomagnetic and rock magnetic as well as geochemical results from Hole 1149A. The Mn/Al ratio highlights intervals that are strongly influenced by diagenetic alteration. These intervals correspond to intervals of large changes in the magnetic mineralogy and composition. Minima in %Ter indicate the position of discrete ash layers in the sediment column. mrs = meters recovered section. B/M = Brunhes/Matuyama boundary, κ = volume susceptibility, B_{cr} = coercivity of remanence, NRM = natural remanent magnetization, ARM = anhysteric remanent magnetization, Ter = terrigenous.

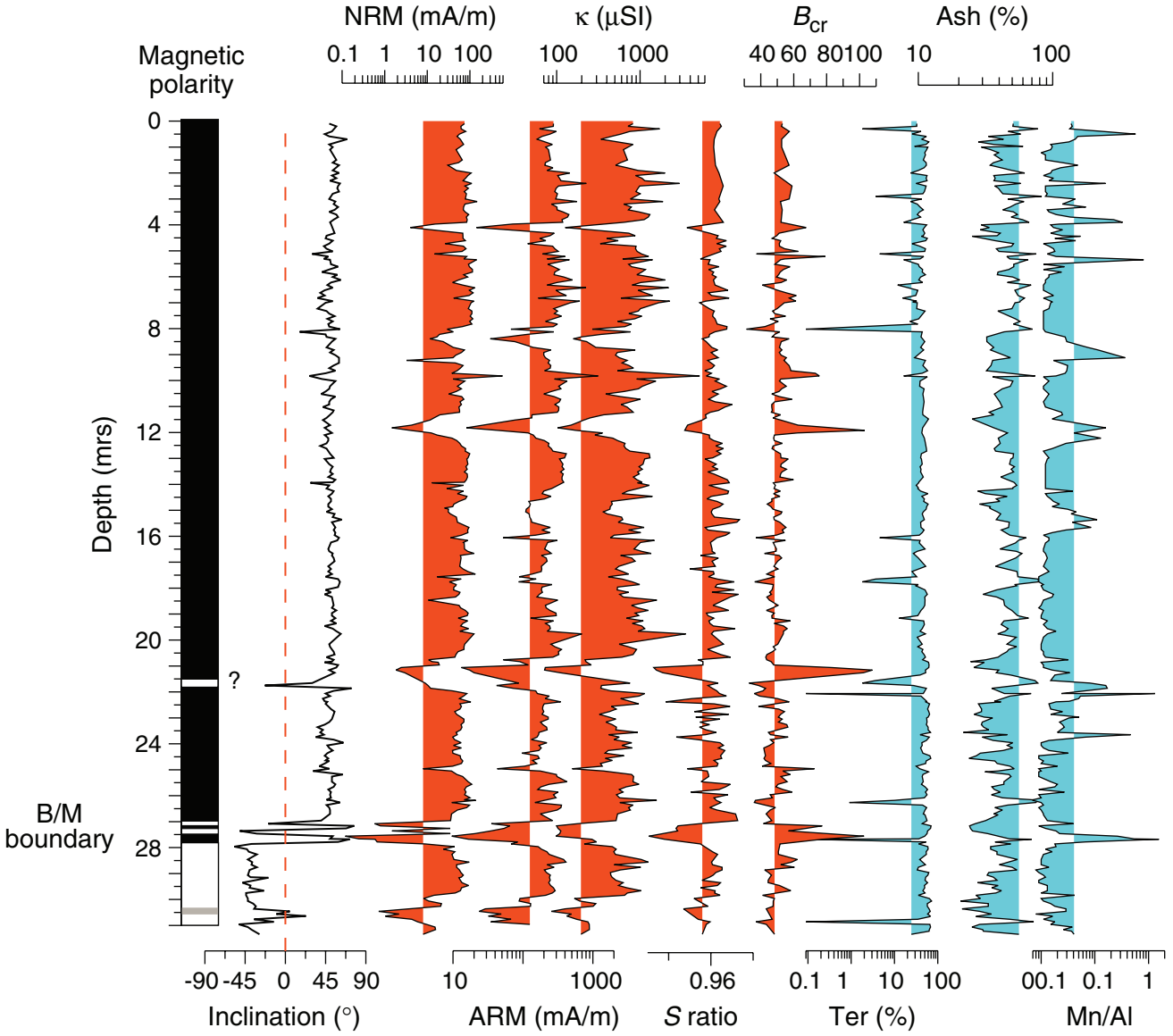

Figure F4. Bivariate scatter plots highlighting the relation between various parameters from Hole 1149A, referred to in the text. Thin lines show respective linear regressions. Dispersed ash and terrigenous dust are inversely correlated. CaO and dispersed ash are positively correlated. Magnetic parameters, here IRM (mA/m), correlate with CaO (wt%). Magnetic concentration-dependent parameters, here anhysteric remanent magnetization (ARM) (mA/m) vs. κ (μSI), yield $R^2 > 0.8$. κ = volume susceptibility, IRM = isothermal remanent magnetization.

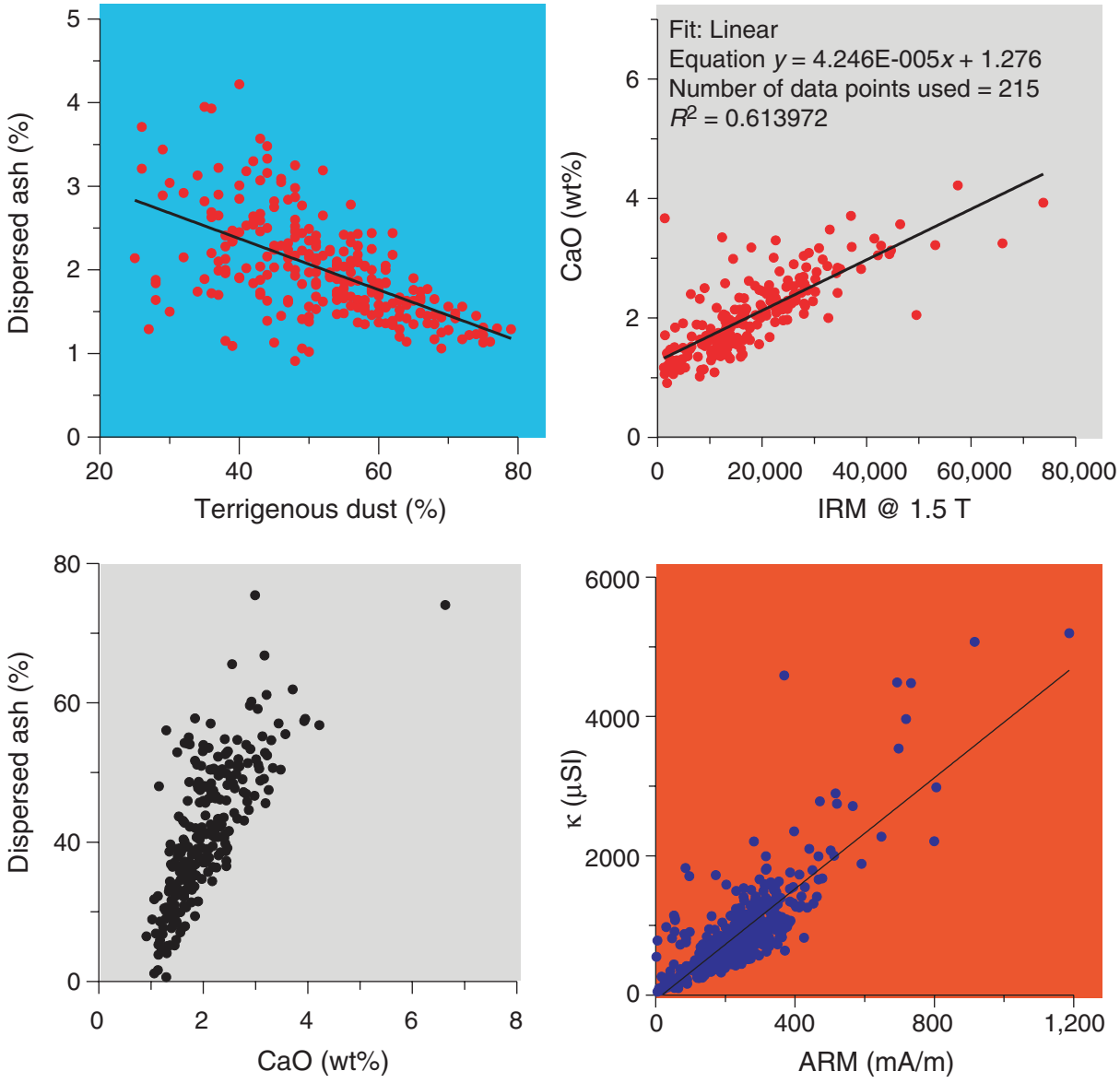

Figure F5. Typical examples of the isothermal remanent magnetization (IRM) acquisition and the backfield measurements for two samples from Hole 1149A (low- and high-coercivity samples).

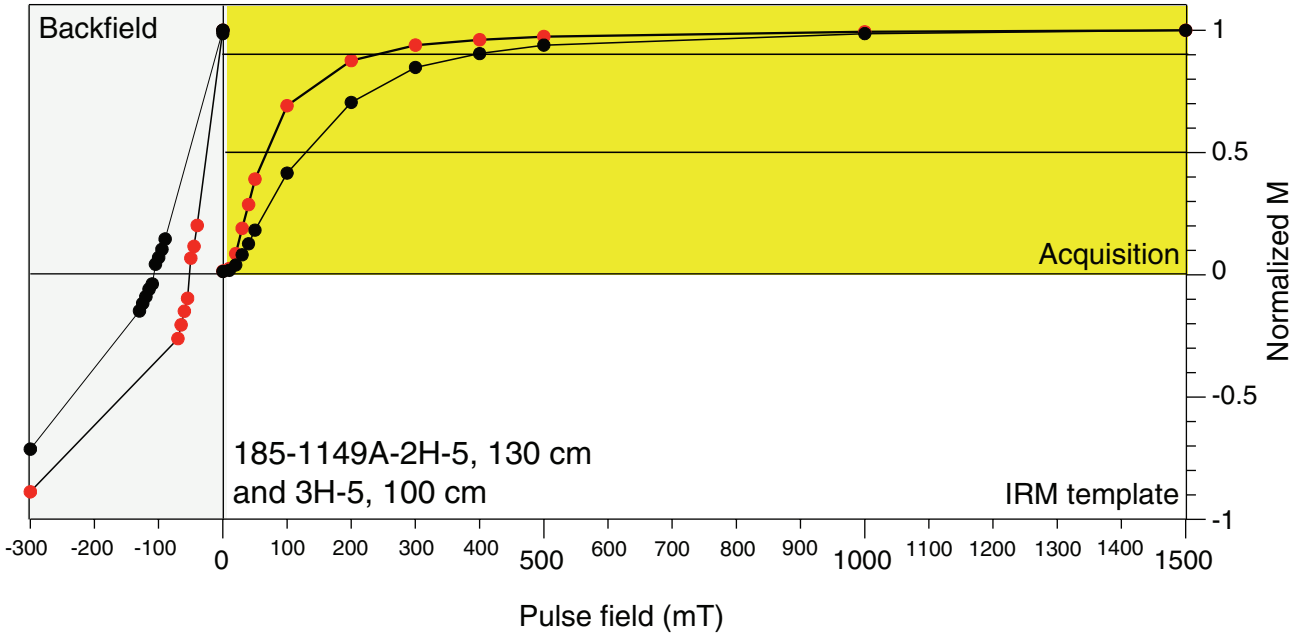

Figure F6. Sample 185-1149A-3H-2, 100 cm, is a typical example of the high- and low-temperature susceptibility measurements from the background sediment, excluding the magnetic low-intensity zones, where the magnetic signal is carried by magnetite. Temp = temperature.

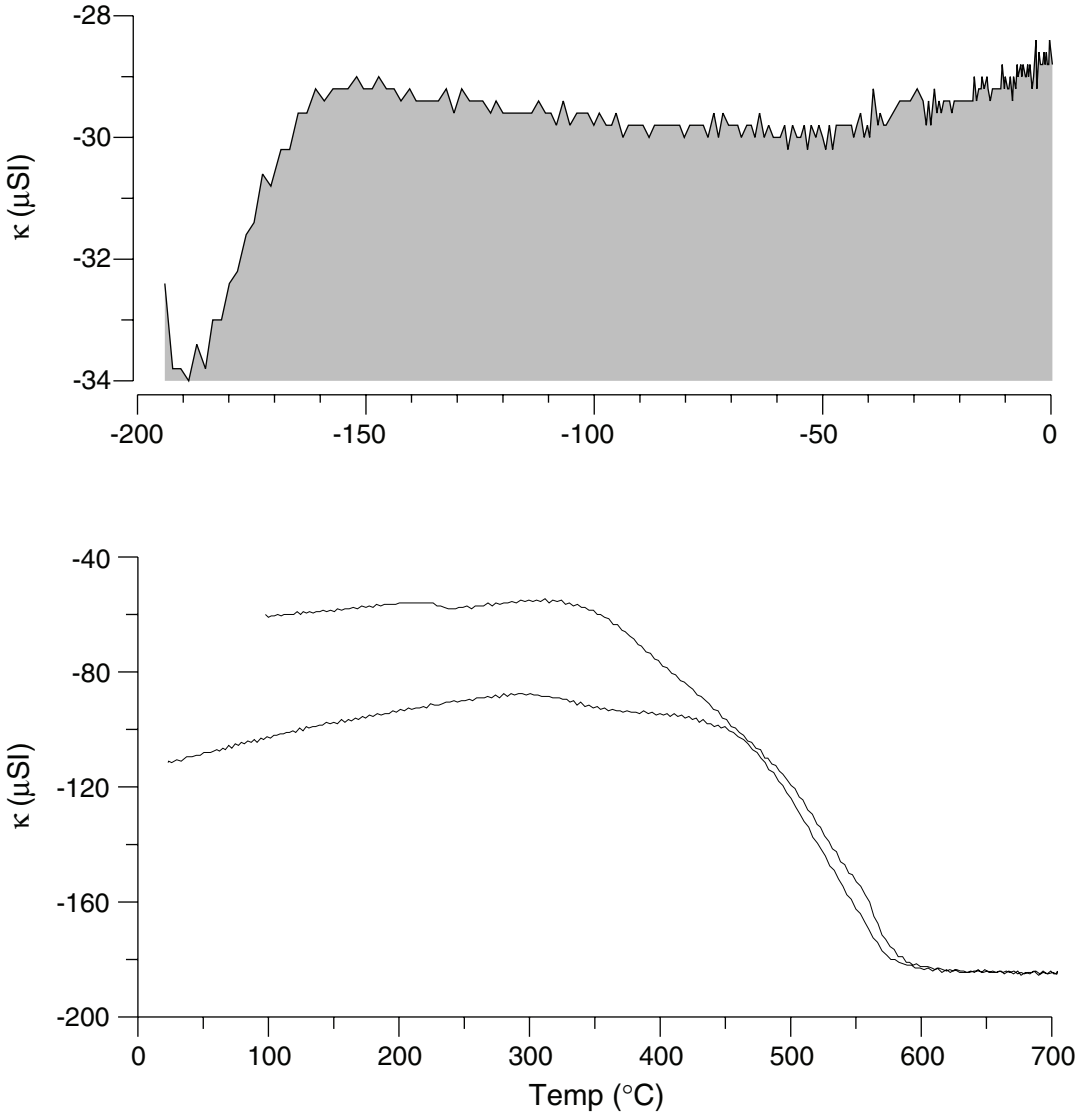

Figure F7. Intensity of the natural remanent magnetization (NRM) (demagnetized with 15-mT AF), inclination, and declination. Declination is not oriented and is arbitrary with respect to geographic north. Declinations near 0° are plotted >360° for graphical reasons. Also shown is the polarity interpretation (Brunhes and Matuyama Chrons) (also see Figure F8, p. 18). Orthogonal vector diagram and AF demagnetization diagram on the right side are a typical example from Hole 1149A. Gray shading = principal position of diagenetic intervals in Hole 1149A. mrs = meters recovered section; ARM = anhysteretic remanent magnetization, B/M = Brunhes/Matuyama.

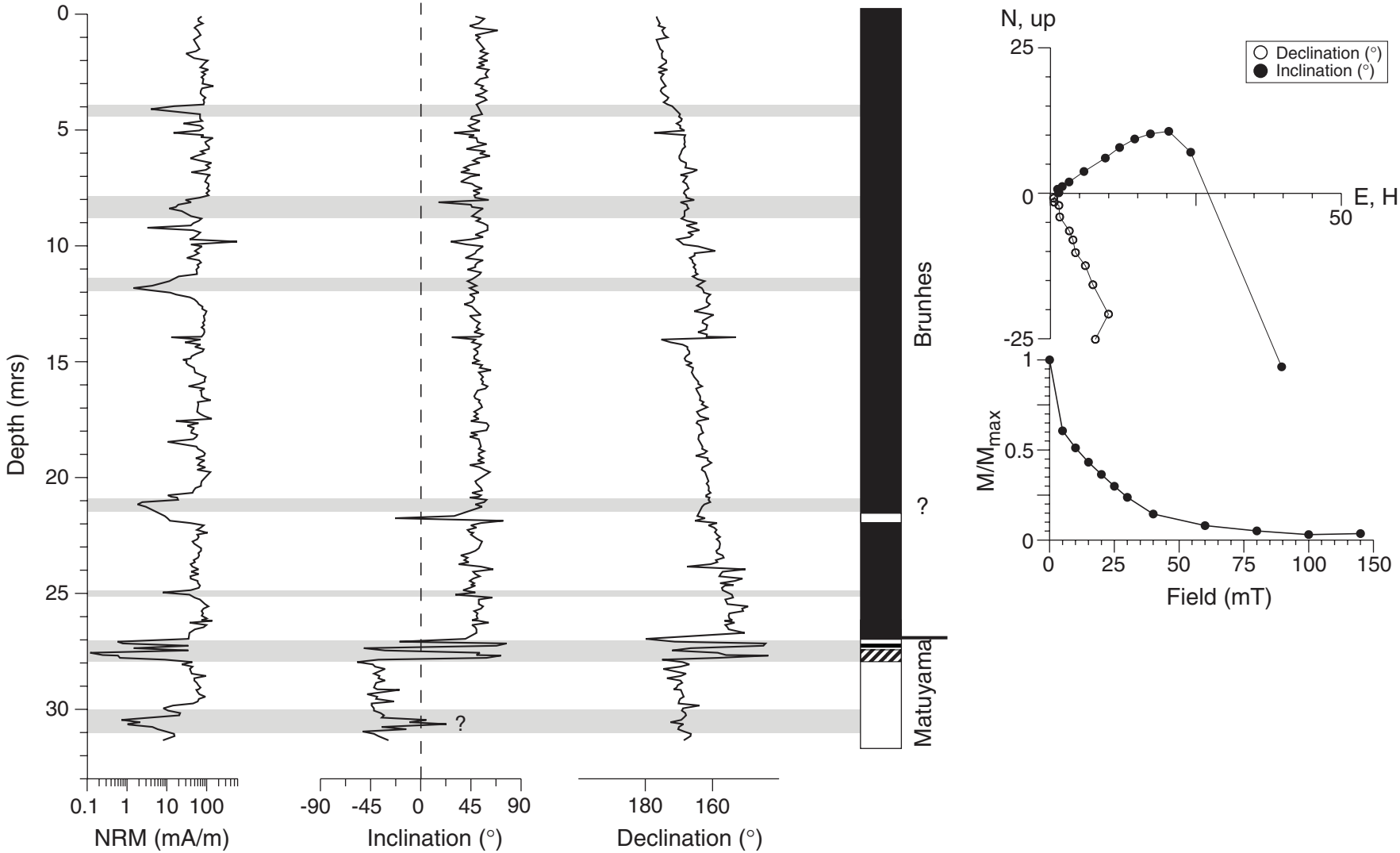

Figure F8. Details of the inclination, anhysteretic remanent magnetization (ARM), and Mn/Al variations across the Brunhes/Matuyama (B/M) boundary (27.04 mrs) in Hole 1149A. Black = normal polarity; white indicates = reversed polarity; crosshatch = partial destruction of the original polarity. Mn peaks are due to rhodochrosite ($MnCO_3$). mrs = meters recovered section.

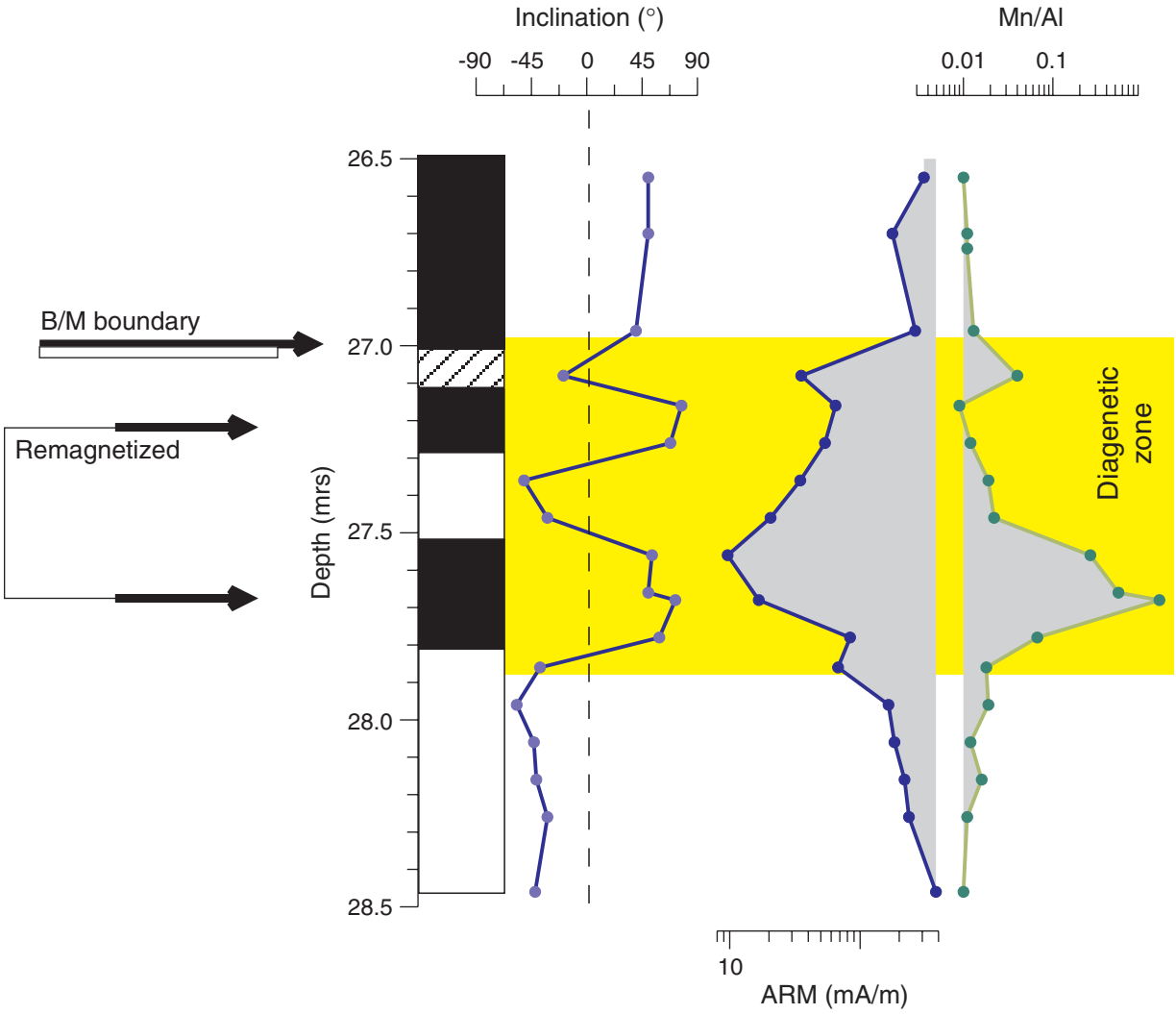

Figure F9. Light shaded curve = spectral analysis of Al; dark shaded curve = discrete ash layers are excluded from the calculation. E = eccentricity bands; O = obliquity bands; P = precession bands. These bands correspond to a sedimentation rate of 3.47 cm/k.y.

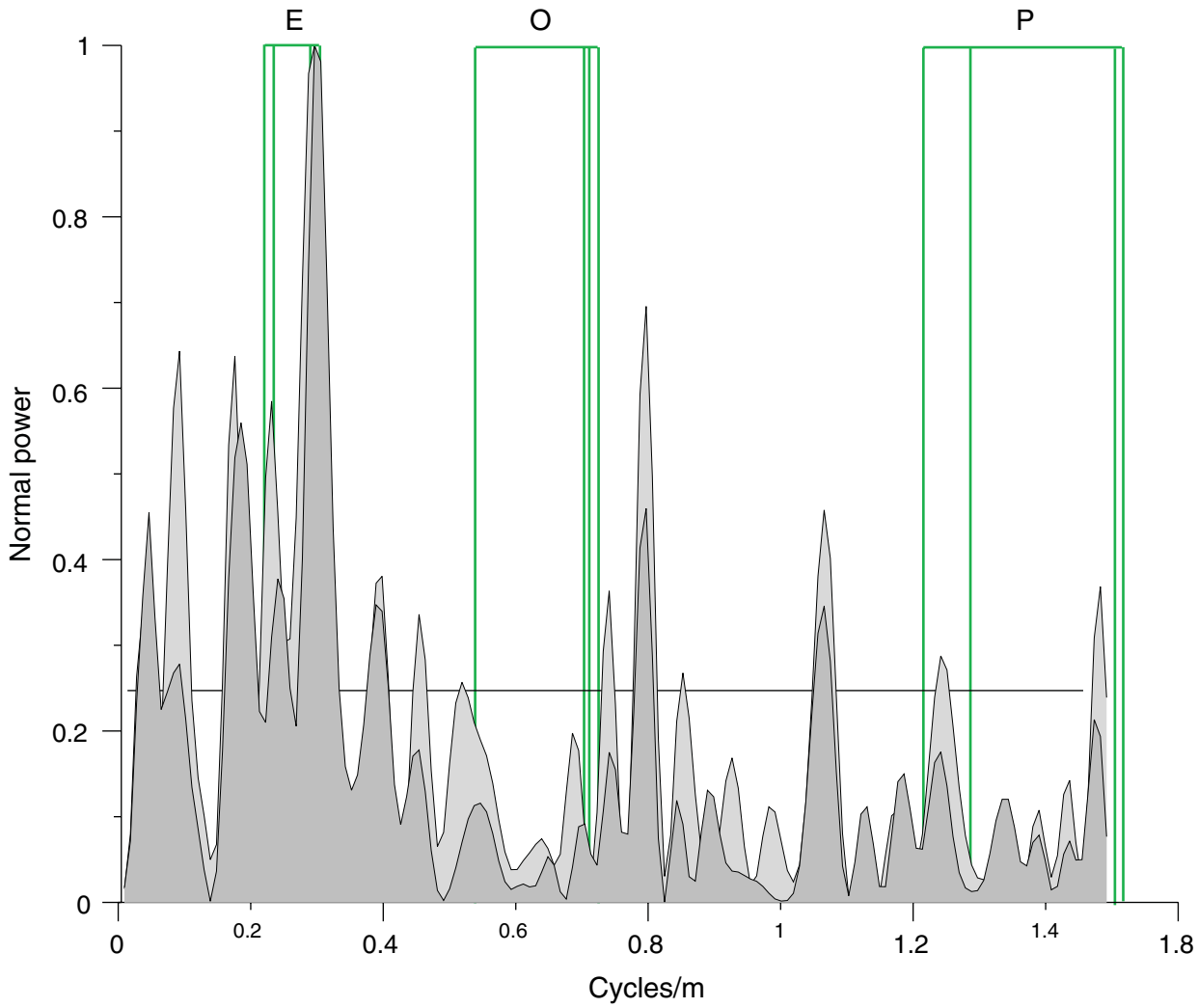

Figure F10. The correlation of the CaO record from Hole 1149A to the SPECMAP stack (Imbrie et al., 1984) is used to convert depth to age. Numbers assigned to the SPECMAP curve indicate respective interglacial stages. Peaks in Cr (ppm) indicate the position of discrete ash layers, further highlighted by the thin vertical lines. Note that the vertical axis increases downward for Cr and CaO (wt%) (highlighted by the black arrow) for graphical reasons. Anhysteretic remanent magnetization (ARM) is shown to highlight intervals of dominant diagenetic alteration. Also see Figure F11, p. 21. B/M = Brunhes/Matuyama boundary.

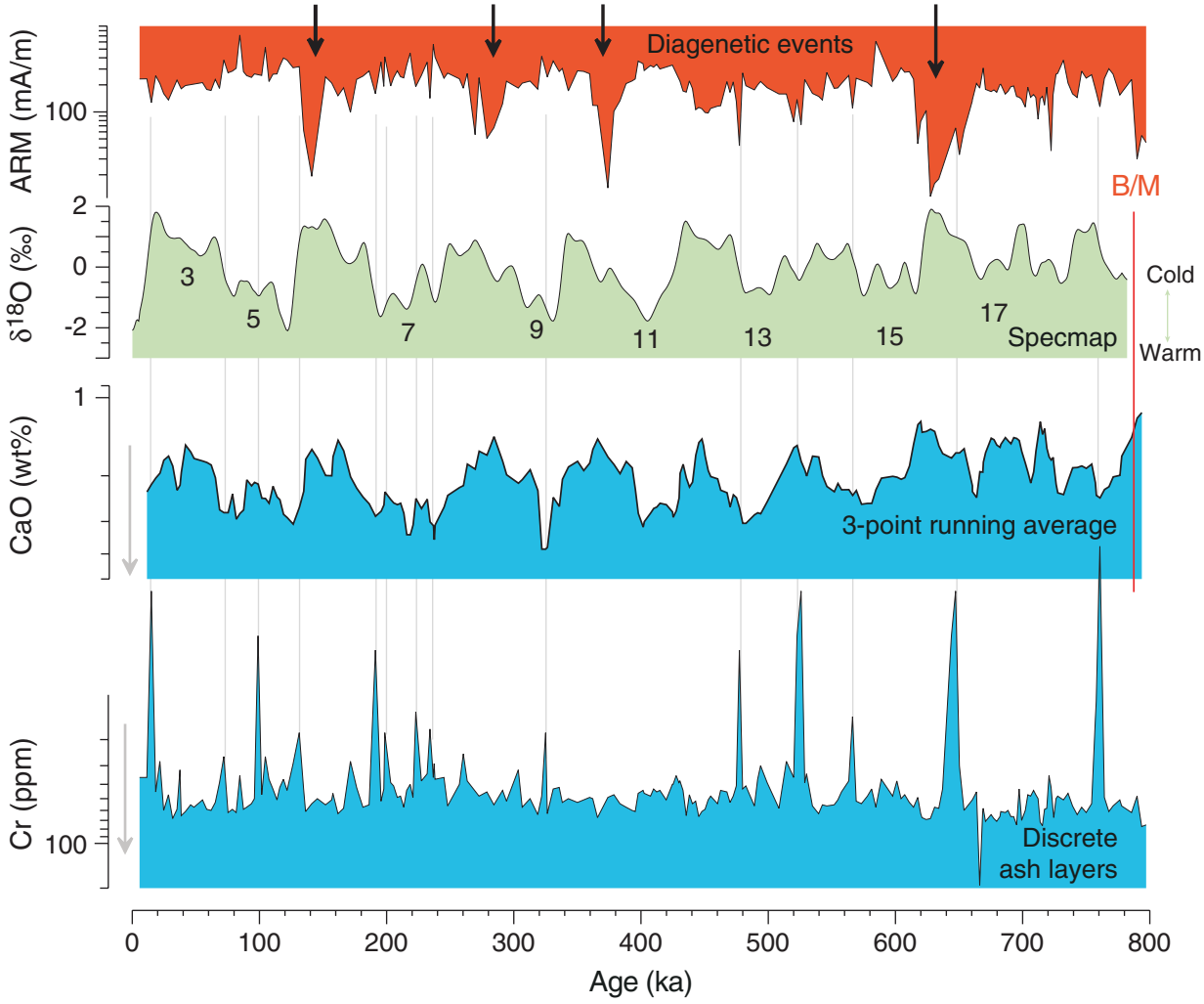

Figure F11. Average sedimentation rates in centimeters per thousand years calculated on the basis of Figure F10, p. 20. Dots = tie points used for the depth/time conversion. SPECMAP (Imbrie et al., 1984) is shown for reference.